A Six Degrees of Freedom Haptic Interface for Laparoscopic Training

Wisdom C. Agboh Mustafa Yalcin Volkan Patoglu

Abstract— **We present the novel kinematics, workspace characterization, functional prototype and impedance control of a six degrees of freedom haptic interface designed to train surgeons for laparoscopic procedures, through virtual reality simulations. The parallel kinematics of the device is constructed by connecting a 3RRP planar parallel mechanism to a linearly actuated modified delta mechanism with a connecting link. The configuration level forward and inverse kinematics of the device assume analytic solutions, while its workspace can be shaped to enable large end-effector translations and rotations, making it well-suited for laparoscopy operations. Furthermore, the haptic interface features a low apparent inertia with high structural stiffness, thanks to its parallel kinematics with grounded actuators. A model-based open-loop impedance controller with feed-forward gravity compensation has been implemented for the device and various virtual tissue/organ stiffness levels have been rendered.**

I. Introduction

Laparoscopy, a commonly used minimally invasive surgical procedure, utilizes slender surgical tools and cameras inserted into the abdomen of a patient through small ports (typically, 5–15 mm in diameter) on the skin, enabling the surgeon to perform numerous procedures without large incisions, as is the case with conventional open surgery. In the recent years, the number of minimally invasive surgical procedures has increased greatly and this approach is currently considered as the preferable surgical procedure for a large number of treatments [16], [24]. In comparison with traditional open surgical procedures, laparoscopy offers reductions in trauma, post-operative pain, recovery time, scarring and blood loss for the patient and is more cost-effective due to the reduced risk of complications, shorter hospital stays and less medication requirements [10], [12].

Despite numerous advantages laparoscopy presents for patients, it is quite difficult to master for surgeons. Unlike the traditional open surgery, during laparoscopy, the surgeon's hand motions are reflected about the incision point, known as the fulcrum effect, access to the patient's body is restricted, and only 2D visual feedback is available resulting in a loss of vital depth perception. Furthermore, laparoscopy instruments have a limited range of motion and haptic/touch information is reduced while using these devices [11], [15].

Due to the difficulty in mastering laparoscopy, surgical training is indispensable and effective training approaches are crucial. Conventionally training involves the use of patients, cadavers and animals. This approach is disadvantageous, since a cadaver neither breathes nor bleeds, animal and human tissues do not possess the same properties and the availability of animals or human cadavers is quite limited for surgical training. In addition, the conventional training does not provide a means to precisely evaluate a surgeon's skill or level of experience [8].

Virtual reality (VR) simulation, where a trainee virtually interacts with human tissue, is a viable alternative to the conventional laparoscopic surgical training, bridging the gap between the learning process and actually carrying out the *in vivo* surgery. VR simulation not only reduces the training costs and number of animal/cadaver experiments, but also makes it possible for the surgical tasks to be repeated as much as required [23].

Even though all VR simulation involve realistic visual feedback, force feedback may not be available. VR simulations without force feedback is disadvantageous, since the surgeon can only acquire skills related to the tool motion without establishing an understanding of the forces required to accomplish such motions in the human body with minimal injury to surrounding tissue. VR surgical trainers without force feedback include the surgeon consoles of daVinci Surgical System [12] and Zeus Surgical System [25].

The incorporation of force feedback into VR simulation enhances the surgeon's perception of pulling and grasping maneuvers, such that surgeons can grasp tissues with less force and without causing scars. Consequently, this improves the trainee's overall performance [22], [26]. In the literature, [1], [3], [13], [20], [29] present master devices with force feedback. These devices possess up to 4 degrees of freedom (DoF) and are considered sufficient under the assumption that the laparoscopic tool is tightly constrained in the abdomen.

Even though constraining the trocar after the initial insertion to only 4 DoF is meaningful for many laparoscopic procedures, the ability to move the trocar location is necessary for the initial tool insertion, as well as to simulate tissue stiffness around the trocar. In particular, during laparoscopy, the trocar is inserted through the incision point which should be at least 50% larger than the trocar diameter [6]. During the initial tool insertion, the trocar is moved within the incision as required to avoid damage to the internal organs. Given that half of the major injuries related to laparoscopy take place due to the initial tool insertion [17], it is crucial for laparoscopic training devices to allow for the translational DoF of the trocar to train surgeons about its placement to minimize insertion related complications. Furthermore, the trocar translations also introduce some flexibility when the incision points are wrongly placed on the abdomen, as small tool translations in these ports can save the surgeon from making extra incisions on the patient's body and increasing

This work has been partially supported by TUBITAK Grant 115M698.

W. C. Agboh, M. Yalcin and V. Patoglu are with the Faculty of Engineering and Natural Sciences at Sabancı University, Istanbul, Turkey. {wisdomagboh,myalcin,vpatoglu}@sabanciuniv.edu

the risk of complications. In addition to training proper trocar placement, the translational degrees of freedom at the incision point can be used to render various tissue stiffness at this interaction point and to estimate the stresses that take place at the incision. Proper control of interaction forces at the incision is important to ensure precise tool control without inducing scaring of the surrounding tissue.

Several six DoF haptic interfaces with serial kinematics, such as Phantom [21] and Virtuose 6D [2], have been employed for laparoscopic training. Even though these devices possess relatively large workspace, they suffer from low stiffness and force output capacity. In particular, the mean and maximum force requirements during laparoscopy are reported as 8.5 N and 68 N, respectively [7], while abdominal wall stiffness can be up to 2.2 N/mm [27]. On the other hand, 6 DoF parallel haptic devices, such as [14], [18], [19], [30], feature small footprint, high force bandwidths, high stiffness, passive backdrivability and low inertia, since their actuators can be grounded. However, none of these haptic interfaces possess a workspace that is well-suited for laparoscopic training.

We present a 6 DoF haptic interface for laparoscopic training. The device features novel parallel kinematics that not only allows for high force control bandwidth through the grounding of all of its actuators, but also possesses a workspace that is well-suited for laparoscopy. In particular, the device has large translation workspace relative to the tool's axis, while it is also capable of performing virtually unlimited roll rotations about this axis. Large stroke is useful for surgical training, since a long tool insertion across the abdomen is required in many cases, such as in hernia repair. Large roll workspace is also crucial, since a 270° roll rotation is needed for driving a needle through a tissue in just a single movement. Eliminating the need for re-grabbing lessens the burden on the surgeon to pay attention to the initial tool configuration during these maneuvers. Furthermore, after the laproscope has been introduced into the abdomen, it needs to be rotated by 360° about its axis, to visually check for bowel injuries by inspecting the tool for any adherent bowels [4].

II. Mechanism Type Selection

Surgical training requires multiple DoF: 4 DoF (for pitch, yaw, roll and tool insertion) are required when the trocar location is fixed and extra two DoF are required for locating the trocar and/or allowing tissue deformations at the incision point. Along these lines, we design a 6 DoF haptic interface, which allows for a large tool translation along and an unlimited rotation about the tool axis.

A fully parallel mechanism is preferred, since these mechanisms possess some inherent advantages over serial mechanisms in satisfying requirements of force feedback applications. In particular, parallel mechanisms offer compact designs with high stiffness and have low effective inertia, since their actuators can be grounded. In terms of dynamic performance, high position and force bandwidths are achievable with parallel mechanisms thanks to their light weight but stiff structure. Furthermore, parallel mechanisms do not superimpose position errors at joints; hence, can achieve higher precision.

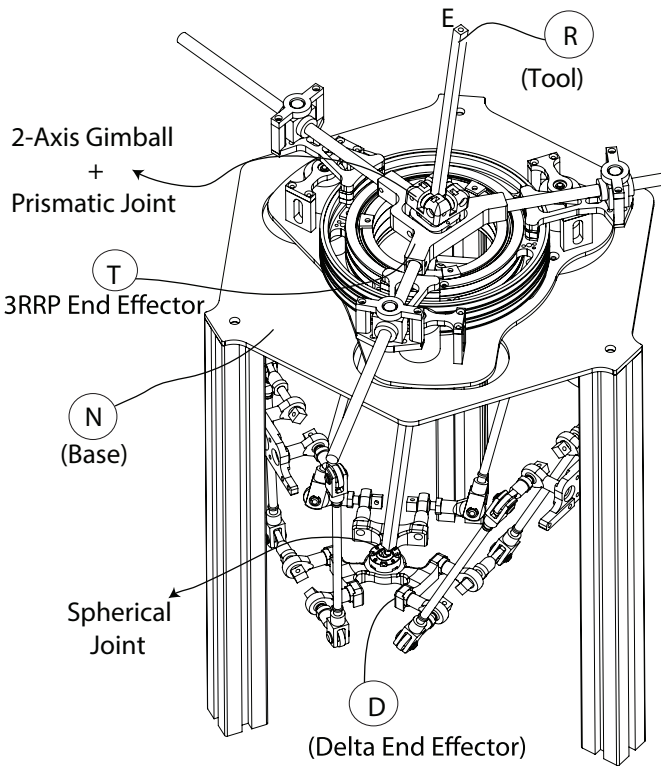

Fig. 1: Kinematics of the device: a linear modified delta mechanism, a 3RRP planar parallel mechanism, and the tool connecting them.

The novel kinematics of the device, is constructed by connecting two 3 DoF parallel mechanisms to achieve the desired tool workspace. In particular, a 3RRP planar parallel mechanisms is connected to a linear modified delta mechanism with the tool, as shown in Figure 1. The end-effector of the delta mechanism can perform 3 DoF translations in space, while the 3RRP mechanism can perform 2 DoF translations and 1 DoF rotation in plane. None of these mechanisms have singularities within their regular workspace. For the underlying kinematics, a linear delta mechanism is chosen, since large tool insertion/retraction can be easily achieved by modifying the linear stroke of the actuators of this mechanism. Similarly, a 3RRP mechanism is preferred, since it can provide virtually unlimited translations in plane, which can be easily mapped to the rotation of the laparoscopic tool about its axis.

To construct the haptic interface in Figure 1, the 3RRP and linear modified delta mechanisms are grounded such that their end-effectors face each other. One end of the tool is attached to the end-effector of the delta mechanism with a spherical joint, such that the location of this end of the tool can be controlled by the delta mechanism. Then, a two axis gimbal in series with a prismatic joint is attached to the end-effector of the 3RRP mechanism, such that the tool can pass through the prismatic joint. This way, the 3RRP mechanism can directly control where the tool intersects the plane of its end-effector, as well as the rotation of the tool about its axis.

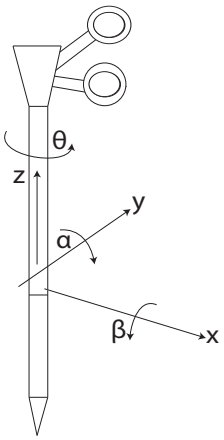

Fig. 2: 6 DoF (x, y, z, roll (θ), pitch (β), yaw (α)) movements of the laparoscopic tool

Figure 2 depicts the 6 DoF movements of the laparoscopic tool. The left/right and forward/backward motions of the tool (trocar) can be controlled by moving both the 3$\underline{\text{R}}$RP and delta mechanisms with an equal amount in parallel planes, while the insertion of the tool can be controlled by translating the delta mechanism in a direction normal to these planes. The rotation of the tool about its own axis (roll) is directly controlled by the rotation of the 3$\underline{\text{R}}$RP, while the left-right (yaw) and forward-backward (pitch) rotations of the tool about the incision point can be controlled by relative movements of the two mechanisms in parallel planes, as depicted in Figure 3.

III. Kinematic Analysis

The kinematics of the haptic device can be derived by studying each of its three main components: the linear modified delta mechanism, the 3$\underline{\text{R}}$RP mechanism and the tool. Each of these components has analytical configuration level forward and inverse kinematics. In particular, the configuration level inverse and forward kinematics of linear delta and 3$\underline{\text{R}}$RP mechanism assume analytical solutions as documented in [5] and [28], respectively. Given the kinematics of these two mechanisms, the inverse and forward kinematics of the proposed device can be analytically derived as follows:

A. Configuration Level Forward Kinematics

For the forward kinematics, the position (x_d, y_d, z_d) of the end-effector of the delta mechanism and the position (x_t, y_t) and orientation (θ_t) of the 3$\underline{\text{R}}$RP mechanism are provided and the orientation of the tool and the position of the tool tip need to be determined. A schematic representation of the tool, together with relevant reference frames and points are presented in Figure 3. Bodies R, T, D, and N represent the tool, the end-effector of 3$\underline{\text{R}}$RP mechanism, the end-effector of the linear delta mechanism and the Newtonian reference frame, respectively. A vector basis is attached to each of these bodies. Point O is fixed in N, while Point A denotes the location where the spherical joint is attached at the end-effector of linear delta mechanism. The tool tip is represented by Point E.

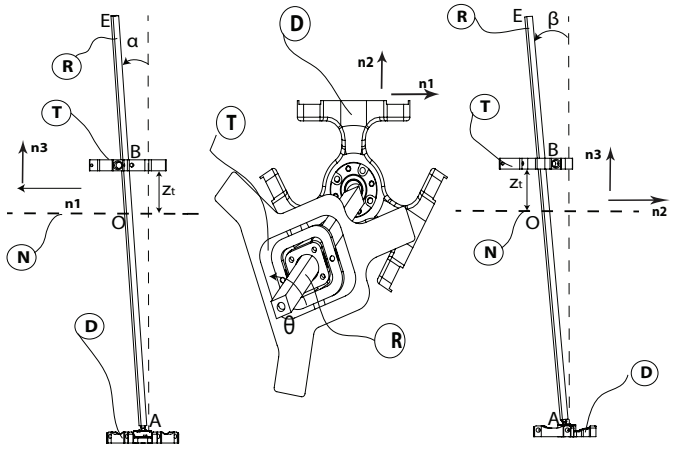

Fig. 3: The relevant bodies and points for kinematic analysis of the connecting link

Let the position vectors from O to A and B be defined as

$$\mathbf{r^{OA}} = x_d\,\mathbf{n_1} + y_d\,\mathbf{n_2} - z_d\,\mathbf{n_3} \quad (1)$$

$$\mathbf{r^{OB}} = x_t\,\mathbf{n_1} + y_t\,\mathbf{n_2} + z_t\,\mathbf{n_3} \quad (2)$$

respectively. A unit vector $\hat{\mathbf{t}}$ along the tool axis can be obtained by normalizing $\mathbf{r^{AB}} = \mathbf{r^{OB}} - \mathbf{r^{OA}}$, while the position vector form O to E is given by $\mathbf{r^{OE}} = \mathbf{r^{AE}} - \mathbf{r^{AO}}$ with $\mathbf{r^{AE}} = l\hat{\mathbf{t}}$, where l denotes the length of the tool. Then,

$$\mathbf{r^{OE}} = x_e\mathbf{n_1} + y_e\mathbf{n_2} + z_e\mathbf{n_3} \quad (3)$$

where

$$x_e = \frac{l(x_t - x_d)}{M} + x_d \quad (4)$$

$$y_e = \frac{l(y_t - y_d)}{M} + y_d \quad (5)$$

$$z_e = \frac{l(z_t + z_d)}{M} - z_d \quad (6)$$

and $M = \left((x_t - x_d)^2 + (y_t - y_d)^2 + (z_t + z_d)^2\right)^{\frac{1}{2}}$.

Let the orientation of the tool R with respect to N be defined by the roll (θ), yaw (α) and pitch (β) rotations as depicted in Figure 2. The roll rotation of the device end-effector is equal to the in plane rotation (θ_t) of the 3$\underline{\text{R}}$RP mechanism. Other rotations can be calculated as

$$\theta = \theta_t \quad (7)$$

$$\alpha = \text{atan2}\left((x_t - x_d), (z_t + z_d)\right) \quad (8)$$

$$\beta = \text{atan2}\left((y_t - y_d), (z_t + z_d)\right) \quad (9)$$

B. Configuration Level Inverse Kinematics

Given the tip position (x_e, y_e, z_e) and orientation (α, β, θ) of the tool, the end-effector position of the delta (x_d, y_d, z_d) and the end-effector position (x_t, y_t) and orientation (θ_t)

$$J_R = \begin{bmatrix} 1+\frac{l(x_d-x_t)^2}{M^3}-\frac{1}{M} & \frac{l(x_d-x_t)(y_d-y_t)}{M^3} & \frac{l(z_t+z_d)(x_d-x_t)}{M^3} & \frac{l((z_t+z_d)^2+(y_d-y_t)^2)}{M^3} & \frac{-l(x_d-x_t)(y_d-y_t)}{M^3} & 0 \\ \frac{l(x_d-x_t)(y_d-y_t)}{M^3} & \frac{1+l(y_d-y_t)^2}{M^3}-\frac{1}{M} & \frac{l(z_t+z_d)(y_d-y_t)}{M^3} & \frac{-l(x_d-x_t)(y_d-y_t)}{M^3} & \frac{l((z_t+z_d)^2+(x_d-x_t)^2)}{M^3} & 0 \\ \frac{-l(z_t+z_d)(x_d-x_t)}{M^3} & \frac{-l(z_t+z_d)(y_d-y_t)}{M^3} & -1+\frac{1}{M}-\frac{l(z_t+z_d)^2}{M^3} & \frac{l(z_t+z_d)(x_d-x_t)}{M^3} & \frac{l(z_t+z_d)(y_d-y_t)}{M^3} & 0 \\ 0 & \frac{-(z_t+z_d)\cos(\alpha)}{k_2} & \frac{y_d-y_t}{k_2} & 0 & \frac{z_t+z_d}{k_2} & -\sin(\alpha) \\ \frac{-(z_t+z_d)\cos(\beta)}{k_1} & 0 & \frac{(x_d-x_t)\cos(\beta)}{k_1} & (z_t+z_d)\cos(\beta)k_1 & 0 & \sin(\beta)\cos(\alpha) \\ \frac{(z_t+z_d)\sin(\beta)}{k_1} & 0 & \frac{-(x_d-x_t)\sin(\beta)}{k_1} & \frac{-(z_t+z_d)\sin(\beta)}{k_1} & 0 & \cos(\alpha)\cos(\beta) \end{bmatrix}$$

where $k_1 = (z_t+z_d)^2+(x_d-x_t)^2$ and $k_2 = (z_t+z_d)^2+(y_d-y_t)^2$.

of the 3RRRP mechanism can be calculated as

$$\theta_t = \theta \quad (10)$$
$$x_t = x_e + \tan(\alpha)(z_t - z_e) \quad (11)$$
$$y_t = y_e + \tan(\beta)(z_t - z_e) \quad (12)$$
$$x_d = \frac{l(c_5)\tan(\alpha)}{c_1(z_e - z_t)} - c_2 \quad (13)$$
$$y_d = \frac{l(c_5)\tan(\beta)}{c_1(z_e - z_t)} - c_3 \quad (14)$$
$$z_d = c_4 - \frac{l(c_5)}{c_1(z_e - z_t)} \quad (15)$$

where

$$c_1 = \tan^2(\alpha)+\tan^2(\beta)+1$$
$$c_2 = \frac{l^2\tan(\alpha)}{c_1(z_e - z_t)} - x_e$$
$$c_3 = \frac{l^2\tan(\beta)}{c_1(z_e - z_t)} - y_e$$
$$c_4 = \frac{l^2}{c_1(z_e - z_t)} - z_e$$
$$c_5 = l + \sqrt{c_1}(z_t - z_e)$$

C. Motion Level Kinematics

Let the angular velocity of the tool R with respect to N be given as ${}^{\mathbf{N}}\omega^{\mathbf{R}} = \omega_{e_x}\mathbf{n_1} + \omega_{e_y}\mathbf{n_2} + \omega_{e_z}\mathbf{n_3}$, while the tip velocity in N is defined as ${}^{\mathbf{N}}\mathbf{v}^{\mathbf{E}} = \dot{x}_e\mathbf{n_1} + \dot{y}_e\mathbf{n_2} + \dot{z}_e\mathbf{n_3}$. The kinematic Jacobian J_R relating end-effector velocities of linear delta and 3RRRP mechanisms to tool velocities can be derived as

$$\begin{bmatrix}\dot{x}_e & \dot{y}_e & \dot{z}_e & \omega_{e_x} & \omega_{e_y} & \omega_{e_z}\end{bmatrix}^T = J_R \begin{bmatrix}\dot{x}_d & \dot{y}_d & \dot{z}_d & \dot{x}_t & \dot{y}_t & \dot{\theta}_t\end{bmatrix}^T \quad (16)$$

where J_R is presented at the top of the page. If J_T and J_D respectively denote the Jacobian of the 3RRRP and the linear delta mechanisms, relating their end-effector velocities to their actuator velocities, the kinematic Jacobian J of the device, characterizing the map between the tool velocities to actuator velocities of linear delta and 3RRRP mechanisms can be derived as

$$J = J_R \begin{bmatrix} J_D & 0 \\ 0 & J_T \end{bmatrix} \quad (17)$$

IV. Workspace Analysis

Figure 4 presents the reachable workspace of the haptic interface for a tool length of 150 mm, a 3RRRP workspace of 60 mm radius and a modified linear delta mechanism with 120 mm stroke. The workspace characterization considers the physical limits of the spherical joint and self collisions of the device.

The workspace of the device can be easily adjusted for a given laparoscopic procedure by performing an optimal dimensional synthesis, where the radius of the 3RRRP mechanism, the stroke and the distal link lengths of the linear delta mechanism are considered as design variables. In particular, the yaw and pitch rotations of the tool can be increased by increasing the radius of 3RRRP and/or modifying the stroke of the linear delta mechanism, as can be deduced from Eqns. (8) and (9).

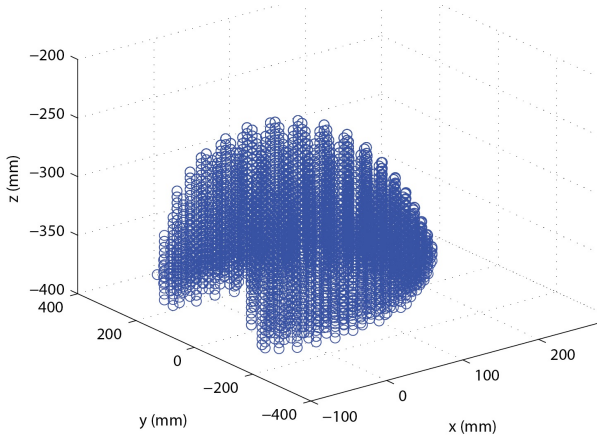

Fig. 4: The reachable workspace of the prototype

V. Implementation

Figure 5 presents a prototype of the laparoscopic haptic interface. The 3RRRP mechanism is constructed utilizing three large diameter, slim, concentric ball bearings. These rings are actuated by grounded, direct drive coreless DC motors coupled to a capstan transmission to achieve low friction and backlash. The large ring diameters help to achieve a large transmission ratio. The mechanism is grounded by a hollow cylinder rigidly attached to the inner rings of the

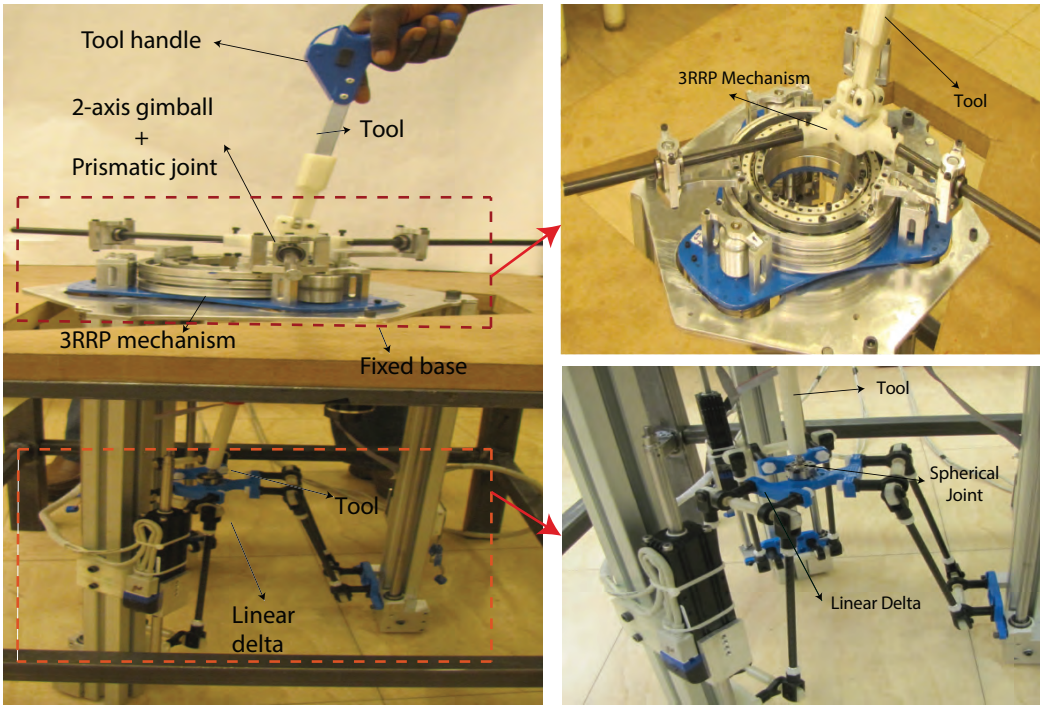

Fig. 5: The force feedback laparoscopic training robot

concentric ball bearings. Even though 3RRP mechanism can provide virtually unlimited rotations, a 480° limit is imposed by the thickness of the rings and the routing of the capstan cables. The center of the mechanism is hollow, which allows the tool to pass through. The symmetric end-effector of the 3RRP mechanism is constructed using three aluminum shafts rigidly connected at their center with a 120° angle between the shafts. A two axis gimbal in series with a prismatic joint is attached to the center of this end-effector.

The linear modified delta mechanism is constructed using carbon fiber links that feature high strength to weight ratio. The delta mechanism is actuated using three direct drive linear motors with embedded encoders. Direct drive actuation minimizes transmission related frictional loss and backlash. All three linear actuators are grounded. A high precision spherical joint is attached to the end-effector of the delta mechanism, which is connected to one end of the tool. The tool is chosen as a slender aluminum rod with a square cross section.

VI. Control and Experimental Evaluation

The prototype is built as an impedance-type device, featuring grounded actuators, high stiffness components, low apparent inertia, and with minimal hard to model parasitic effects, such as friction and backlash. Consequently, an open loop impedance controller with feed-forward gravity compensation is implemented for real-time control of the device.

To evaluate the control performance of the device, several virtual fixtures along x and y directions of the tool have been rendered as linear springs with stiffness ranging from that of a typical soft tissue to a cartilage type tissue in the human body. Figure 6 presents force-deflection data measured for these renderings, by applying known forces to the laparoscopic tool at the virtual incision point and measuring its displacement. Best linear fits on the data are also presented.

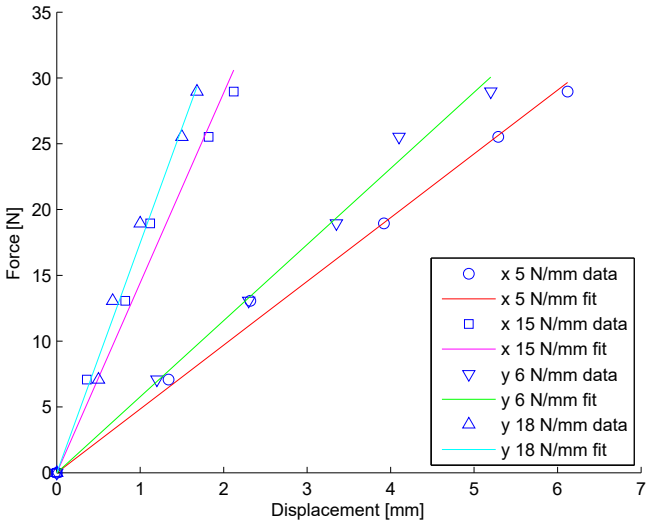

Fig. 6: Virtual fixtures along x and y directions

Table I presents R^2 value characterizing the quality of the line fit, the slope of these lines, and the rendering error. These results indicate that even under open loop impedance control (without force feedback), the device can achieve high fidelity impedance renderings with RMS errors less than 4%.

To evaluate the trajectory tracking performance of the device, a chirp signal with a 40 mm amplitude and frequencies increasing up to 1 Hz is applied as the reference motion along the axis of the tool. Figure 7 presents a sample plot demonstrating the chirp signal tracking performance of the

TABLE I: Spring rendering results for the device

Axis	Desired stiffness [N/mm]	Slope of fitted line [N/mm]	Rendering error [%]	Quality of fit (R^2)
x	5	4.9	3.0	0.993
x	15	14.4	3.8	0.974
y	6	5.8	3.7	0.992
y	18	17.5	3.0	0.988

device. The RMS error for this trajectory tracking task is calculated as 0.3%, indicating that the impedance controller can also achieve good motion tracking performance.

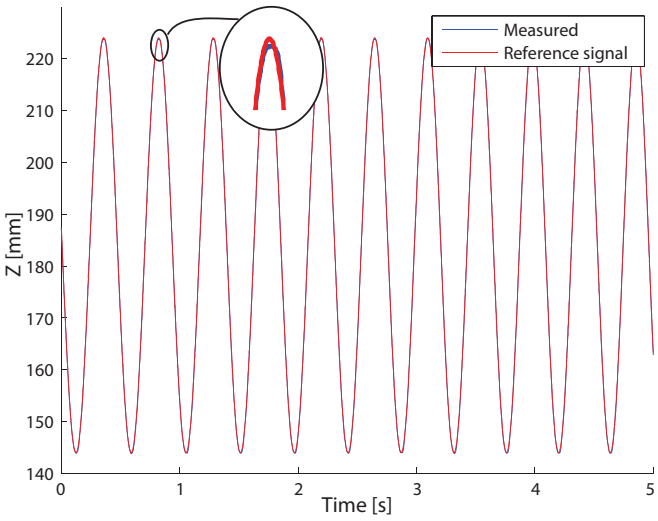

Fig. 7: Trajectory tacking performance of the device under impedance control

VII. Conclusion and Future Work

We have presented the kinematics, workspace characterization, functional prototype and real-time impedance control of a novel 6 DoF haptic interface designed for laparoscopic training. The device features parallel kinematics that assume analytical solutions. The kinematics also allows of all actuators to be grounded to archive low apparent inertia at the tool. An impedance-type device has been implemented through use of direct drive actuation and capstan transmission to ensure low friction and backlash, and open loop impedance control performance of the device has been shown to be adequate for haptic simulations.

Ongoing studies include optimal dimensional synthesis of the device [9] and experimental evaluation of the effectiveness of the device during laparoscopic training, especially to investigate the importance of stiffness rendering around the incision point for training trocar placement procedures.

References

[1] Force dimension inc. http://www.forcedimension.com. Accessed 2015.

[2] Haption. http://www.haption.com. Accessed 2015.

[3] Novint. http://www.novint.com. Accessed 2015.

[4] Royal college of obstetricians and gynacologists: Preventing entry-related gynaecological laparoscopic injuries. http://bsge.org.uk/guidelines.php. Accessed 2015.

[5] Williams R.L II."The Delta Parallel Robot: Kinematics Solutions", Internet Publication. www.ohio.edu/people/williar4/html/pdf/DeltaKin.pdf. 2015.

[6] R. Alberto, B. Renaud, and E. C. Baldo. *Manual of Laparoscopic Urology*. Springer-Verlag Berlin Heidelberg, 2008.

[7] J. Brown, J. Rosen, L. Chang, M. Sinanan, and B. Hannaford. Quantifying Surgeon Grasping Mechanics in Laparoscopy Using the Blue Dragon System. *Stud Health Technol Inform.*, 98:34–36, 2004.

[8] J. Dankelman, M. Chmarra, E. Verdaasdonk, L. Stassen, and C. Grimbergen. Fundamental aspects of learning minimally invasive surgical skills. *Minim Invasive Ther Allied Technol*, 14(4):247–56, 2005.

[9] A. Erdogan, B. Celebi, A. C. Satici, and V. Patoglu. AssistOn-Ankle: A reconfigurable ankle exoskeleton with series-elastic actuation. *Autonomous Robotics*, 2016.

[10] T. Frank, G. Hanna, and A. Cuschieri. Technological aspects of minimal access surgery. *Proc. of the Institution of Mechanical Engineers, Part H: Journal of Engineering in Medicine*, 211(2):129–144, 1997.

[11] A. Gallagher, N. McClure, J. McGuigan, K. Ritchie, and N. Sheehy. An ergonomic analysis of the fulcrum effect in the acquisition of endoscopic skills. *Endoscopy*, 30(7):617–20, 1998.

[12] G. S. Guthart and J. K. Salisbury. The intuitivetm telesurgery system: overview and application. In *Robotics and Automation, 2000. Proceedings. ICRA '00. IEEE International Conference on*, volume 1, pages 618–621 vol.1, 2000.

[13] R. Hendrix, N. Rosielle, and H. Nijmeijer. Design of a haptic master interface for robotically assisted vitreo-retinal eye surgery. In *International Conference on Advanced Robotics*, pages 1–6, 2009.

[14] V. M. Hung and U. J. Na. Tele-operation of a 6-DOF serial robot using a new 6-DOF haptic interface. In *IEEE International Symposium on Haptic Audio-Visual Environments and Games*, pages 1–6, 2010.

[15] D. Jones, J. Brewer, and N. Soper. The influence of three-dimensional video systems on laparoscopic task performance. *Surg Laparosc Endosc*, 6(3):191–7, 1996.

[16] M. W. Khan and M. M. Aziz. Experience in laparoscopic cholecystectomy. *Mymensingh Medical Journal: MMJ*, 19(01):77–84, 2010.

[17] S. Krishnakumar and P. Tambe. Entry Complications in Laparoscopic Surgery. *J Gynecol Endosc Surg*, 1(1):4–11, 2009.

[18] S. U. Lee and S. Kim. Analysis and Optimal Design of a New 6 DOF Parallel Type Haptic Device. In *IEEE/RSJ International Conference on Intelligent Robots and Systems*, pages 460–465, 2006.

[19] G. Long and C. Collins. A pantograph linkage parallel platform master hand controller for force-reflection. In *IEEE International Conference on Robotics and Automation*, pages 390–395 vol.1, 1992.

[20] A. Ma and S. Payandeh. Analysis and Experimentation of a 4-DOF Haptic Device. In *Symposium on haptic interfaces for virtual environment and teleoperator systems*, pages 351–356, 2008.

[21] T. H. Massie and J. K. Salisbury. The PHANToM haptic interface: A device for probing virtual objects. In *ASME Dynamic Systems and Control Division*, pages 295–301, 1994.

[22] G. Picod, A. Jambon, D. Vinatier, and P. Dubois. What can the operator actually feel when performing a laparoscopy? *Surg Endosc*, 19(1):95–100, 2005.

[23] L. Rifat. *Establishing telemedicine in developing countries: From inception to implementation*. IOS Press, Amsterdam, 2004.

[24] T. N. Robinson and G. V. Stiegmann. Minimally Invasive Surgery. *Endoscopy*, 36(01):48–51, 2004.

[25] Russel A. Faust. *Robotics in surgery : history, current and future applications*. Nova Science Publishers, New York, 2007.

[26] G. Tholey, J. Desai, and A. Castellanos. Force Feedback Plays a Significant Role in Minimally Invasive Surgery - Results and Analysis. *Ann Surg*, 241(1):102–109, 2005.

[27] D. Tran, F. Podwojewski, P. Beillas, M. Ottenio, D. Voirin, F. Turquier, and D. Mitton. Abdominal wall muscle elasticity and abdomen local stiffness on healthy volunteers during various physiological activities. *Journal of the Mechanical Behavior of Biomedical Materials*, 60:451 – 459, 2016.

[28] M. Yalcin and V. Patoglu. Kinematics and design of AssistOn-SE: A self-adjusting shoulder-elbow exoskeleton. In *IEEE/RAS/EMBS International Conference on Biomedical Robotics and Biomechatronics*, pages 1579–1585, 2012.

[29] T. Yang, J. Liu, W. Huang, L. Yang, C. K. Chui, M. H. Ang, Y. Su, and S. K. Y. Chang. *Frontiers of Intelligent Autonomous Systems*, chapter Mechanism of a Learning Robot Manipulator for Laparoscopic Surgical Training, pages 297–308. Springer Berlin Heidelberg, 2013.

[30] J. Yoon and J. Ryu. Design, fabrication, and evaluation of a new haptic device using a parallel mechanism. *IEEE/ASME Transactions on Mechatronics*, 6(3):221–233, 2001.